

3D printing of MAX/PLA filament: Electrochemical in-situ etching for enhanced energy conversion and storage

Shaista Nouseen^{a,b}, Kalyan Ghosh^b, Martin Pumera^{a,b,c,d,*}

^a Quantum Materials Laboratory, 3D Printing & Innovation Hub, Center for Nanorobotics and Machine Intelligence, Department of Chemistry and Biochemistry, Mendel University in Brno, Zemedelska 1, Brno 61300, Czech Republic

^b Future Energy and Innovation Laboratory, Central European Institute of Technology, Brno University of Technology, Purkynova 123, Brno 61200, Czech Republic

^c Advanced Nanorobots and Multiscale Robotics Laboratory, Faculty of Electrical Engineering and Computer Science, VSB - Technical University of Ostrava, 17. listopadu 2172/15, Ostrava 70800, Czech Republic

^d Department of Medical Research, China Medical University Hospital, China Medical University, No. 91 Hsueh-Shih Road, Taichung, Taiwan

ARTICLE INFO

Keywords:

Electrochemical etching
MXenes
MAX
3D printing
Electrode
Hydrogen evolution reaction
Supercapacitor

ABSTRACT

Two-dimensional (2D) MXenes are promising materials for a variety of sustainable energy-related applications such as photoelectrochemical water splitting and energy storage devices. Among the MXene family, the $Ti_3C_2T_x$ is mostly prepared by selective etching of Al from the Ti_3AlC_2 MAX phase using hydrofluoric acid (HF) or in-situ produced HF as an etchant. However, the severe toxicity, handling of HF acid as well as the oxidation and degradation of freshly synthesized MXenes when stored as aqueous suspensions obstruct the large-scale production of MXenes. 3D printing is an innovative and versatile technology utilized for a plethora of applications in the field of energy applications. Thus, integration of 3D printing technology with the synthesis procedure of MXene will provide a new outlook for large-scale production and the long-storing capability of MXene. Herein, we fabricated a novel MAX (Ti_3AlC_2)/poly(lactic acid) (PLA) filament for fused deposition modeling (FDM) 3D printing followed by etching of the 3D-printed MAX/PLA electrode into 3DP-etched-MAX employing chronoamperometry technique consecutively in 9 M HCl and 4 M NaOH as electrolytes. The 3D printed electrochemically etched MAX (3DP-etched-MAX) electrode shows promising behaviour for the photoelectrochemical hydrogen evolution reaction (HER) and capacitive performance. In general, this work demonstrates a path of production of large-scale manufacturing of MAX/PLA filament and 3DP-etched-MAX electrodes without using toxic HF for energy conversion and energy storage applications. This work paves the way to fabricate other novel MAX filaments and electrodes for several applications beyond energy conversion and storage.

1. Introduction

The incessant growth of the human population induced extreme consumption of fossil fuels and impacted living environmental conditions. In addition to the current state of energy crises, climate change, environmental issues, and excessive cost of fuels concern the scientific community [1,2]. Thus, addressing these concerns and finding an alternate source of energy is paramount for the researcher. Research in the field of electrochemical energy conversion and storage devices (EECS) has emerged as the green, sustainable, and inexpensive pathway to develop an alternate source of energy [1,3,4]. To enhance the performance of the material utilized for energy conversion such as Hydrogen evolution reaction (HER), and storage devices like

supercapacitors, extensive efforts have been dedicated for designing and developing advanced functional materials by combining various materials and technologies [5–7].

The 3D-printing technology led to the mass-scale production of lightweight, flexible designs and cost-effective electronic devices and components for a disparate range of potential applications in the field of EECS [8,9]. In the 3D printing technique computer-aided design (CAD) models are used to produce complex 3D objects easily. 3D printing of electrodes allows a wide range of properties such as rigidity, flexibility, size, shape, and geometry [9–11]. Among different 3D printing techniques, the FDM technique represents an eco-friendly and fast prototyping technology in the fabrication of EECS devices. In the FDM process, a filament is printed layer-by-layer to obtain the preferred

* Corresponding author at: Quantum Materials Laboratory, 3D Printing & Innovation Hub, Center for Nanorobotics and Machine Intelligence, Department of Chemistry and Biochemistry, Mendel University in Brno, Zemedelska 1, Brno 61300, Czech Republic.

E-mail address: pumera.research@gmail.com (M. Pumera).

<https://doi.org/10.1016/j.elecom.2023.107652>

Received 11 October 2023; Received in revised form 15 December 2023; Accepted 16 December 2023

Available online 29 December 2023

1388-2481/© 2023 The Authors. Published by Elsevier B.V. This is an open access article under the CC BY license (<http://creativecommons.org/licenses/by/4.0/>).

geometry of the devices. Thermoplastic polymers such as poly lactic acid (PLA), acrylonitrile butadiene styrene (ABS), acrylonitrile styrene acrylate (ASA), polyethylene terephthalate glycol (PETG) based filaments are commonly used for FDM printing. Numerous precursors such as activated carbons, carbon nanotubes (CNTs), graphite, graphene, transition metal dichalcogenides (TMDs), metal oxides and other electroactive compounds have been utilized in the polymer matrix to fabricate conductive filament for 3D-printing to apply in electrochemical applications [9,12–20]. MXenes have attracted significant attention as a promising candidate for EECS devices due to their exceptional properties such as high electrical conductivity, porosity, and hydrophilicity [11,21–24]. Recently, several research groups reported MXenes-based electrodes for energy applications with different 3D printing technology [14,25–28]. MXene is synthesized from its parental MAX phase. MXene is represented with a general formula $M_{n+1}X_nT_x$ and the MAX is presented as $M_{n+1}AX_n$ where M stands for a transition metal, A is group 13 elements, X is carbon or nitrogen and T is surface functional group such as F, –OH. The selective etching of the ‘A’ element from MAX derived the MXene. So far, direct use HF and *in situ* generated HF are found as the most efficient etchant to derive MXene [21,29–33]. However, HF is highly toxic and corrosive with potentially lethal outcomes. Additionally, the stabilization of MXene in an aqueous solution is a crucial problem due to its oxidation and hydrolysis [34–36]. Thus, there is a high demand for HF-free methodology for MXenes synthesis [29,30,37–39].

Recently, several groups also reported fluoride-free strategies for the synthesis of MXenes from the MAX phase [40–42]. Besides, researchers reported a few critical findings for MXene synthesis following the routes such as electrochemical etching of MAX in HCl [43,44], electrochemical etching MAX using LiOH and LiCl aqueous solution [45], alkali-treated conversions of MAX into MXene [46], binary solutions treated MAX into MXenes [47], halogens etch MAX into MXenes [48], chemical vapor deposition of carbides [49] element replacement approach for the conversion of MAX into MXene [50], and Lewis acid etching for preparing MXenes [51]. Among these techniques, electrochemical etching was found to be promising to use for MXene synthesis in energy storage applications. However, the preparation of MXene from such an electrochemical etching process is tedious and it lacks large-scale fabrication.

To tackle this issue herein, we report a large-scale fabrication of a 3DP MAX electrode employing the FDM 3D printing technique followed by HF-free electrochemical etching. A bespoke MAX/PLA filament was fabricated optimizing the ratio of Ti_3AlC_2 MAX followed by FDM 3D-printing technology to prepare a bespoke MAX/PLA filament. The MAX/PLA filament was 3D-printed to obtain electrodes for electrochemical etching using the chronoamperometry technique in a two-step process utilizing 9 M HCl followed by 4 M NaOH as electrolyte solutions. This work provides a new route to the synthesis of fluoride-free and stable 3DP-etched-MAX electrodes. The 3DP-etched-MAX electrodes can easily be applied directly for HER and supercapacitor applications as free-standing working electrodes without the need for an additional current collector.

2. Experimental section

2.1. Materials

Polyethylene glycol (PEG, Mn 1000 g mol⁻¹), lithium chloride (LiCl), and H₂SO₄ were purchased from Sigma-Aldrich, Germany, Polylactic acid (PLA, Ingeo biopolymer 2003D) was procured from Nature Works LLC, USA. Dichloromethane (DCM), HCl, and NaOH were purchased from Penta, Czech Republic. MAX (Ti_3AlC_2) powder was procured from Y-Carbon, Ukraine. The electrolytes were prepared with deionized water with resistivity resistivity > 18 MΩ cm.

2.2. MAX filament fabrication

The MAX filament was fabricated following two-step procedure. In the first step, thick film of MAX/PLA about a thickness of ≈ 3–4 mm was prepared. In this process, a slurry was prepared first by dissolving PLA in DCM solvent with a ratio of 0.1 g mL⁻¹ in a beaker. The beaker was sealed tightly with a parafilm to avoid evaporation of DCM at room temperature. This solution was stirred constantly until the PLA granules were dissolved and a clear solution was observed. Later, a plasticizer of PEG was added to the above solution in a mass ratio of 4 % to PLA and stirred thoroughly until it dissolved. Next, MAX was added to the solution and continuously stirred for 2 hrs until a homogeneous slurry was obtained. The amount of MAX was taken as 10 % mass ratio to the PLA. The slurry was then poured into glass petri dishes, which was considered to obtain an approximate film thickness of about ≈ 3–4 mm. The Petri dishes were kept overnight under a fume cupboard to evaporate the solvent at room temperature and dried completely. A solid film was formed which was peeled off from the petri dish. The films were cut into small pieces of ≈ 4 × 4 × 4 mm³ for extrusion purpose. In the second step, the above-cut small pieces were fed into the extruder (Felfil Evo, Italy) to extrude the filament. The extruder barrel and nozzle temperature were kept at ≈ 180–185 °C and a screw speed of ≈ 8–9 rpm to extrude the filament with uniform thickness. The extruded filament was simultaneously wound in a spool attached to the winding setup. The filament diameter was controlled to ≈ 1.7 mm by maintaining the screw rpm and the spool pulling speed.

2.3. 3D printing of electrodes

The printing of electrodes was carried out utilizing a 3D printer (Prusa i3 MK3, Czech Republic). Firstly, the electrodes were designed employing the software Autodesk Fusion 360. The .stl drawing file is sliced via Prusa Slicer software (version 2.5.0) and exported as the G-code file. The G-code file was printed operating a Prusa i3 MK3 FDM printer (Prusa Research, Czech Republic) equipped with an Olsson ruby-tipped 0.6 mm nozzle (3DVerkstan, Sweden). The temperature of the nozzle was kept at 225 °C and bed temperature of 60 °C during 3D printing. The 3D-printed MAX/PLA electrodes were then activated in 4 M NaOH to remove the surface PLA as reported in our previous work [52]. The activated electrode is denoted as 3DP MAX.

2.4. Electrochemical etching of 3DP MAX electrodes

To etch the 3DP MAX electrodes, the chronoamperometry technique was employed using 9 M HCl applying a potential of 5 V for 30 min using 3DP MAX as the working electrode, graphite as the counter electrode, and Ag/AgCl (1 M KCl) as reference electrode a potentiostat PGSTAT 204 (Metrohm Autolab, Netherlands) equipped with Nova 2.1 software. The electrode was taken out and washed several times with DI water. The electrode was further treated in 4 M NaOH electrolyte following the same conditions in the chronoamperometry technique. After that, the electrode was washed again several times with DI water and dried at room temperature. The etched electrode is denoted as 3DP-etched-MAX.

2.5. Photoelectrochemical measurement

The linear sweep voltammetry (LSV) technique was utilized to analyze the photoelectrochemical behaviour of the 3DP MAX and 3DP-etched-MAX electrodes for HER employing the same potentiostat as mentioned in the previous section. Here, the Ag/AgCl (1 M KCl) was used as a reference electrode, graphite as the counter electrode, and a 3D printed electrode as the working electrode in 0.5 M H₂SO₄ electrolyte the scan rate of 5 mV s⁻¹ is provided. A customized setup of light-emitting diodes (LEDs, LZ4–44UV00 and LZ4–40B208 LedEngin Inc.) is employed for the light irradiation source for photoelectrochemical measurements at the wavelengths centred at 365 and 460 nm,

respectively. The photo-electrochemical measurements were carried out utilizing 0.5 M H₂SO₄ as an electrolyte with a scan rate of 5 mV s⁻¹ in a three-electrode system employing linear sweep voltammetry (LSV). The potential (V vs Ag/AgCl) was converted to potential in a reversible hydrogen electrode (RHE) following the previous report with equation $E_{RHE} = E_{Ag/AgCl} + E_{Ag/AgCl}^0 + 0.059 \times \text{pH}$ [3]. Furthermore, the capacitance behaviour of 3D-printed electrodes was evaluated utilizing cyclic voltammetry (CV) and galvanostatic charge–discharge (GCD). The setup utilized was similar to the three-electrode system for HER and 1 M LiCl was utilized as an electrolyte. The areal capacitance value C_d is calculated from Equation S2 as stated in Supporting Information.

2.6. Material characterization

The surface morphology of the 3D-printed electrodes was carried out on the scanning electron microscope (SEM, FEI VERIOS 460 L). The elemental mapping of the various elements present on the material on the 3D printed surface along with the element spectra was obtained by using the EDX detector attached along with the SEM TESCAN LYRA 3 operating at an accelerating voltage of 5–25 kV. Further, to better understand the chemical composition and bonding environment of the 3D printed electrode X-ray photoelectron spectroscopy (XPS, Kratos AXIS Supra) is utilized. The XPS spectra of the electrodes were further calibrated against C 1s peak (285 eV) by using CasaXPS software. The Rigaku SmartLab 3 kW X-ray diffractometer is utilized for X-ray diffraction (XRD) analysis. Following Bragg-Brentano geometry using Cu K α radiation ($\lambda = 0.15418$ nm) which operates at a voltage of 40 kV and a current of 30 mA. UV–visible spectroscopic studies were conducted utilizing a UV–vis spectrophotometer (JASCO V-750). 3DP MAX and 3DP-etched-MAX printed electrode samples are carefully attached to a small glass slide with double-sided tape for the measurements. The surface resistivity of the 3DP MAX and 3DP-etched-MAX electrodes is measured via a multimeter device using a two-probe system. The probe is kept on the electrode surface in five different positions to determine

average values.

3. Results and discussions

In this study, a bespoke MAX/PLA filament was fabricated for FDM printing optimizing the amount of polymer PLA, electroactive material Ti₃AlC₂ MAX and plasticizer PEG. The filament was 3D-printed in a designed shape that is convenient for electrochemical characterization as shown in Fig. S1 in Supporting Information. The 3D-printed MAX/PLA electrode was activated first using 4 M NaOH for ≈ 2.5 h to remove the surface PLA which resulted in a nascent MAX surface for electrochemical etching. The chronoamperometry technique was employed to etch the Al layer from the Ti₃AlC₂ MAX phase. A schematic presentation of the filament preparation, 3D-printing, electrochemical etching process is presented in Fig. 1. Here, two-step procedure was followed to etch the Al layer, in the first step the electrode was treated in 9 M HCl for 30 min applying a constant potential of 5 V followed by rinsing with the deionized water several times. In the second step, the electrode was further treated with 4 M NaOH solution applying the same constant potential of 5 V. The chronoamperometry data for both steps are shown in Figs. S2 and S3 in Supporting Information. The high concentration of Cl⁻ ions in electrolytes reacts with the Al of Ti₃AlC₂ yielding AlCl₃ due to the strong interactions between the Cl⁻ and Al metal [53]. This reaction starts the etching process, however, the newly formed AlCl₃ blocks etch further the inner layer of the Ti₃AlC₂. In the second step, while it was treated with 4 M NaOH, the AlCl₃ was removed and further etching process progressed by reacting Al with OH⁻ ions that form Al(OH)₃ and AlOOH [46,50,54]. The etching equations of reactions are stated below as previously reported by Chen et al. [45].

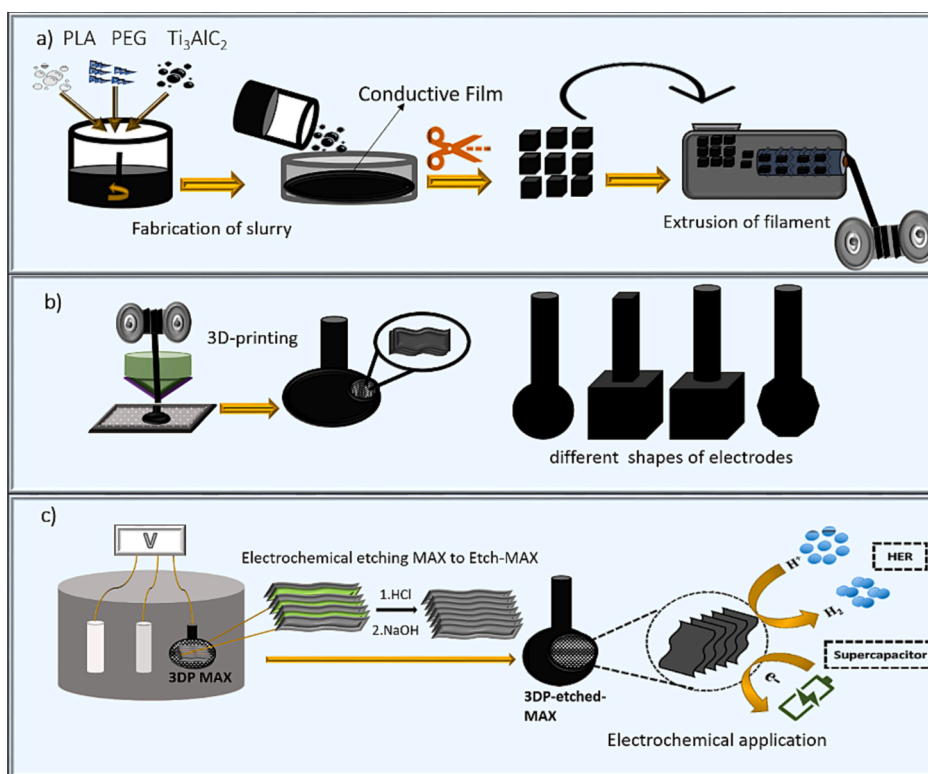
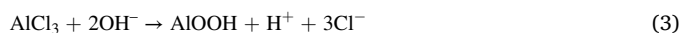
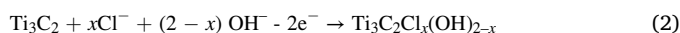


Fig. 1. Schematic illustration of (a) the fabrication of MAX filament and (b) 3D printing of electrodes followed by (c) electrochemical etching of 3DP MAX into 3DP-etched-MAX electrode and electrochemical application in the photoelectrochemical hydrogen evolution reaction and supercapacitor application.

A scanning electron microscopy study was carried out to obtain the surface morphology of the 3D-printed electrodes denoted as 3DP MAX and 3DP-etched-MAX electrodes. The SEM image in Fig. 2a–c shows the surface morphology of the 3DP MAX electrode. It shows that after the removal of the surface PLA from MAX/PLA, MAX phases are open at the surface. The magnified images are shown in Fig. 2b,c which confirm the typical compact layered morphology of the MAX phase. The SEM images in Fig. 2d–f show the surface morphology of the 3DP-etched-MAX electrode that is obtained after electrochemical etching of the 3DP MAX electrode. The magnified images in Fig. 2e,f depict the aluminium etched layers of the 3DP-etched-MAX electrode similar to MXenes.

To have better understanding of the etching process, EDX was carried out for 3DP MAX and 3DP-etched-MAX electrodes. Fig. 3 depicts the EDX spectra displaying the presence of the constituent elements of the 3DP MAX and 3DP-etched-MAX electrodes such as Ti, Al, C, and O. The atomic percentage of the constituent elements from the EDX analysis are listed in Table 1. The percentage of Al in MAX (2.59 %) is reduced to (1.40 %) after the etching process. The EDX mapping of the 3DP MAX and 3DP-etched-MAX electrode are shown in Fig. S4 in Supporting Information which further confirms the etching of the MAX phase.

To comprehend the crystalline structure of the 3DP MAX and 3DP-etched-MAX electrodes, XRD pattern was analyzed. The full diffractogram of the XRD measurement for the 2θ from 5 to 80° is shown in Fig. 4a. The XRD analysis was carried out employing X'pert HighScore software reports. The peak positions at the 2θ of 5–80° corresponding to the d -spacing associated with the crystalline plane. The 3DP MAX electrode shows the same crystalline peaks as reported in the literature [46,50]. In Ti_3C_2 MXene the peak of interest is located for 2θ of 5–10° which is shown in Fig. 4b. The 3DP MAX electrode shows the characteristic peak at 2θ of 9.64° corresponding to the (002) plane with a d -spacing of ≈ 9.16 Å whereas the 3DP-etched-MAX electrode shows a peak at 2θ of $\approx 8.94^\circ$ with a d -spacing of ≈ 9.88 Å. The peak shifting of $\approx 0.70^\circ$ with an increase of d -spacing ≈ 0.72 Å confirms the etching of the MAX phase and conversion of MAX to MXene-like delaminated structure at the surface of the electrode. As this is an etching process of a 3D printed electrode of MAX, it is difficult to etch the core MAX of the electrode. Here, the surface of the 3D electrode which is in contact with the electrolyte is etched.

XPS analysis was carried out to confirm the presence of elements and confirm the etching of Al. In Fig. 4c the wide spectra of the 3DP MAX and 3DP-etched-MAX electrodes clearly show the peaks corresponding to the O 1s, Ti 2p, and C 1s elements at ≈ 529 , 456, and 284 eV, respectively.

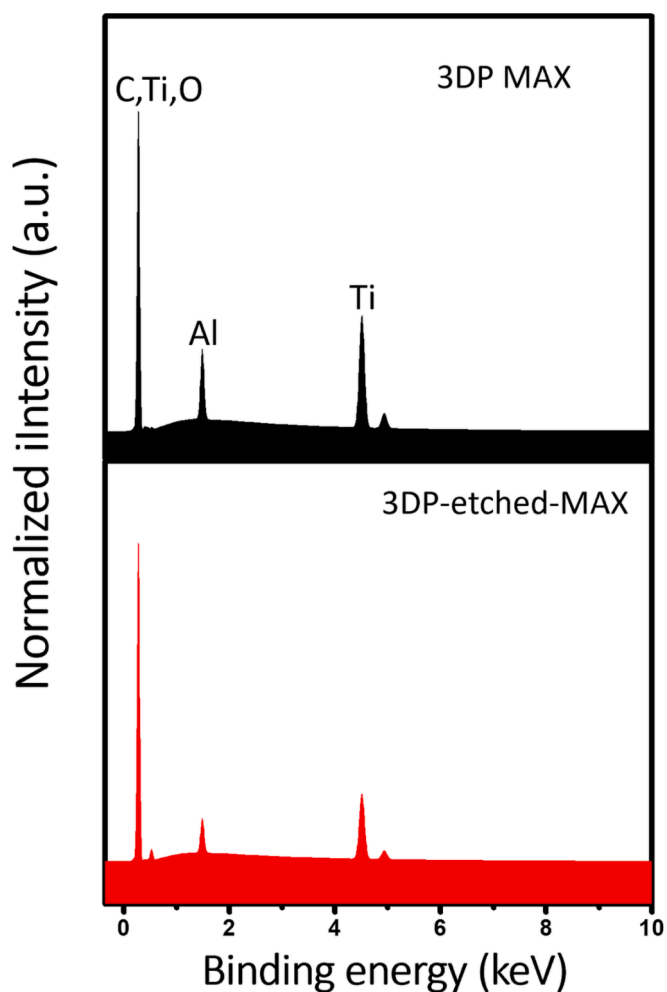


Fig. 3. EDX spectra of 3DP MAX and 3DP-etched-MAX electrodes.

From the wide spectra, the specific region for the binding energy of Al 2p is depicted in Fig. 4d. The Al 2p peak corresponding to the binding energy of ≈ 73 eV disappeared in the 3DP-etched-MAX electrode which again confirms the etching of Al at the electrode surface. The atomic

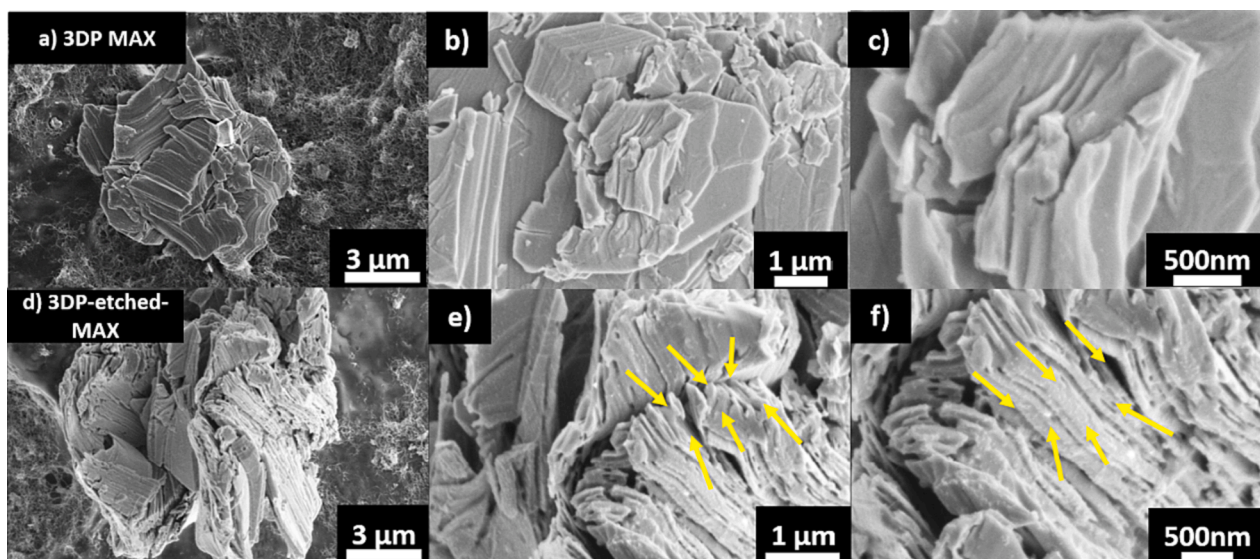


Fig. 2. Scanning electron microscopy (SEM) images. 3DP MAX electrode (a) at low magnification and (b,c) at high magnification; 3DP-etched-MAX electrode (d) at low and (e,f) at high magnification.

Table 1

Elemental percentage of 3DP MAX and 3DP-etched-MAX electrodes from EDX spectra.

Samples	Atomic composition (%)			
	Ti	Al	C	O
3DP MAX	11.19	2.59	85.37	0.86
3DP-etched-MAX	7.32	1.40	84.76	6.52

percentage of the elements from the XPS wide spectra is shown in [Table S1 Supporting Information \[37–47,50–64\]](#). The surface resistivity of the 3DP MAX and 3DP-etched-MAX electrodes are found to be ≈ 550 and $\approx 250 \Omega \text{ cm}$, respectively. UV spectra analysis was also carried out

to determine the active wavelength region for the 3DP-etched-MAX electrode. The 3DP-etched-MAX shows a peak between 300 and 400 nm which is previously reported for MXene as shown in [Fig. S5](#) which unravels its photo-active behaviour [65,66].

The electrochemical active surface area (ECSA) of the 3DP MAX and 3DP-etched-MAX electrodes are calculated as explained in [Supporting Information Fig. S6](#). The ECSA of 3DP MAX and etched-MAX electrodes are found to be ≈ 10.1 and $\approx 26.5 \text{ cm}^2$, respectively. The higher ECSA of the 3DP-etched-MAX electrode is attributed to the removal of the Al layers by the electrochemical etching process.

[Fig. 5a](#) represents the LSV plots of 3DP MAX and 3DP-etched-MAX electrodes for photo-electrochemical HER. The 3DP-etched-MAX shows a better HER response than the 3DP MAX electrode. This is due

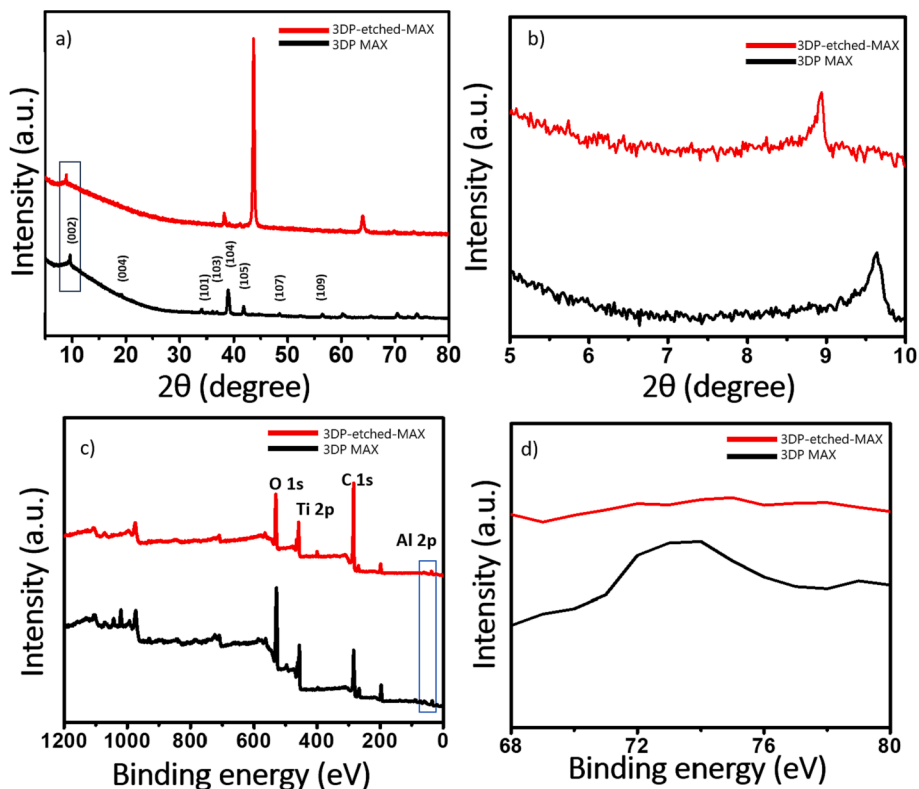


Fig. 4. X-ray diffraction (XRD) patterns of 3D-printed 3DP MAX and 3DP-etched-MAX electrodes (a) the whole 2θ region, and (b) the region of interest from 2θ of 5° to 10° . XPS wide spectra of 3DP MAX and 3DP-etched-MAX electrodes (c) whole region of binding energy and (d) at the region of binding energy of Al.

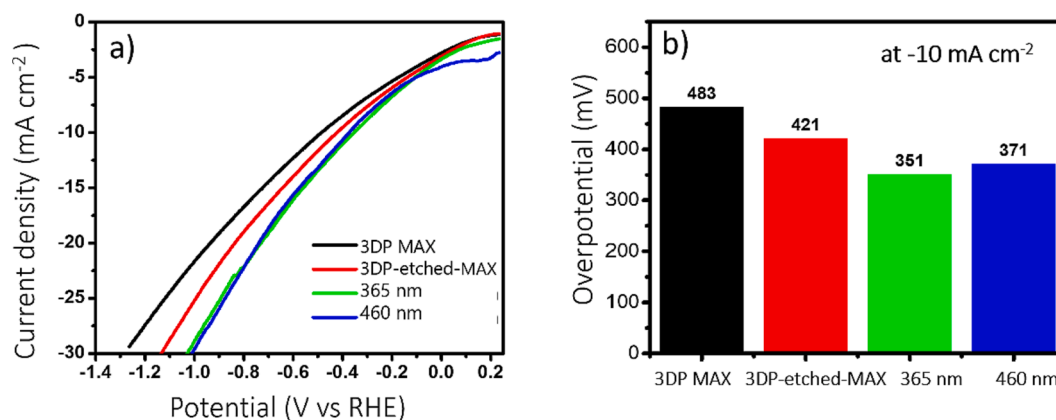


Fig. 5. (a) Photoelectrochemical hydrogen evolution reaction (HER) for 3DP MAX and 3DP-etched-MAX electrodes with light and without light radiations through a source of light with wavelength 365 nm and 460 nm, electrolyte: $0.5 \text{ M H}_2\text{SO}_4$, scan rate 5 mV s^{-1} in a three-electrode setup. (b) The overpotential values selected from figure (a) are shown in the form of a bar graph at current density -10 mA cm^{-2} .

to the formation of the conductive, higher electrochemically active MXene-like surface after electrochemical etching of the 3D electrode. Besides, based on the UV-spectral response, the 3DP-etched-MAX was further studied for photo-electrochemical HER illuminating light radiations at wavelengths of 365 and 460 nm. A better photoelectrochemical HER response was noticed at the wavelength of 365 nm. The photo-electrochemical response was not significantly affected after changing the illumination wavelength from 365 to 460 nm. To better illustrate the variation of photo-electrochemical response of the electrodes, a bar graph is plotted in Fig. 5b, comparing the overpotentials at the current density -10 mA cm^{-2} . The 3DP MAX electrode shows an overpotential of 483 mV while the 3DP-etched-MAX electrode shows 421 mV. Overpotentials of ≈ 351 and ≈ 371 mV were observed illuminating the 3DP-etched-MAX at the wavelength of 365 and 460 nm, respectively. This confirms that the photoelectrochemical HER response is higher for light illumination at the wavelength of 365 nm.

Besides, to better elucidate the photo-responsive behaviour of the 3DP-etched-MAX electrode chronoamperometry study was carried out applying a constant potential of -0.50 V vs. RHE . The electrode was illuminated with continuous light radiations by switching on and off the light radiation. The current density profile of the 3DP-etched-MAX electrode with light illumination 365 and 460 nm is shown in Fig. 6. The current density profile confirms the photo-assisted response in HER. The difference in photo-responsive behaviour is visible in Fig. 6, which indicates that light illumination at the wavelength of 365 nm results in better photochemical activity. When the light is illuminated on the surface of the 3DP-etched-MAX electrode, it converts the incident photons to electron-hole pairs. The reduction of the proton to hydrogen (H_2) is assisted via the electrons that are excited to the conduction band. The above outcomes suggest that the 3DP-etched-MAX electrode can perform both electro- and photo-catalysed HER.

The 3DP MAX and 3DP-etched-MAX electrode electrodes were further employed to study their energy storage capability in a three-electrode test system as a free-standing supercapacitor electrode. Firstly, cyclic voltammetry studies were carried out on 3DP MAX and 3DP-etched-MAX electrodes with a potential window of -0.3 to $+0.5 \text{ V}$ at the scan rates from 5 to 100 mV s^{-1} in 1 M LiCl electrolyte as shown in Fig. 7a,b, respectively. The 3DP-etched-MAX electrode shows a higher current response than the 3DP MAX electrode. A comparison of the CV plots between 3DP MAX and 3DP-etched-MAX electrodes is shown in Fig. 7c. The 3DP-etched-MAX electrode shows a higher enclosed $I-V$ area than the 3DP MAX due to its etched surface that possesses a higher electrochemical active surface area. The conductivity of the 3DP-etched-MAX electrode was also enhanced after the etching process which effects the capacitive performance. Employing similar conditions, GCD measurement was performed on 3DP-etched-MAX electrodes at the same potential window of -0.3 to $+0.5 \text{ V}$ as shown in Fig. 7d. The GCD studies demonstrate the symmetric charging and discharging pattern when lowering the applied current, charge-discharge time was increased. The areal capacitances (C_a) were calculated to be ≈ 40.36 , ≈ 29.92 , and $\approx 8.15 \text{ mF cm}^{-2}$ at the current densities of 1.01, 1.52 and 2.29 mA cm^{-2} , respectively. At low current density, the electrolyte can penetrate the inside core of the electrode, which raises the accessible surface area for the electrolyte ions and increases the capacitive value.

The electrochemical impedance spectroscopy (EIS) study was conducted for the 3DP MAX and 3DP-etched-MAX electrode to analyze their intrinsic charge transfer response. The Nyquist plots of 3DP MAX and 3DP-etched-MAX electrodes within the frequency region of 1 MHz–0.01 Hz are shown in Fig. 8. In the Nyquist plot, at the starting point of the plot, where it intersects with the X-axis, represents the equivalent series resistance R_s , which includes solution resistance, intrinsic resistance of the electrode, and interfacial resistances. The semicircle region followed after R_s represents the charge transfer resistance R_{ct} . Applying the Randles circuit model as depicted in Fig. 8 inset, it is found that the 3DP MAX exhibits very high R_s and R_{ct} of ≈ 1237.5 and $\approx 971.6 \Omega$, respectively as compared to 3DP-etched-MAX which shows the R_s and R_{ct} of \approx

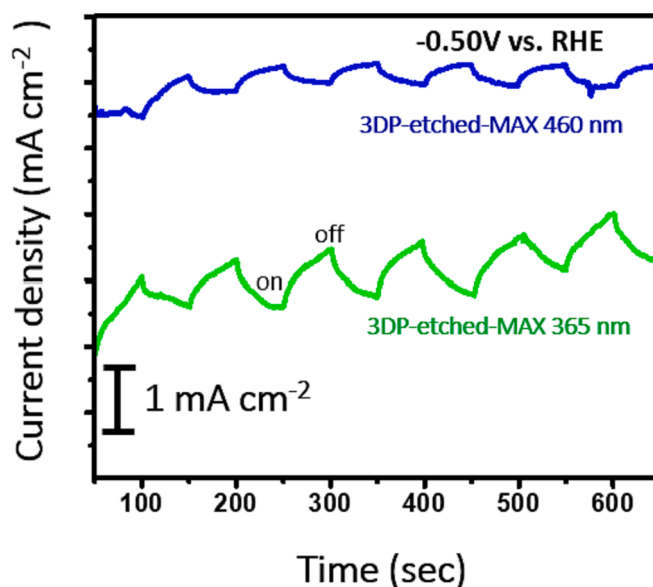


Fig. 6. Chronoamperometry measurements for the illustration of the photo-responsive behaviour towards hydrogen evolution reaction (HER) for 3DP-etched-MAX electrode without and with light radiations through a source having wavelength 365 and 460 nm. 0.5 M H_2SO_4 is used as an electrolyte and constant potential of $-0.50 \text{ V vs. reversible hydrogen electrode (RHE)}$ is applied.

244.5 and $\approx 602.6 \Omega$, respectively. The lower R_s of 3DP-etched-MAX signifies that intrinsic resistance decreased dramatically after the etching process, while the conductivity of the electrode increased. This corroborates with the resistivity data as mentioned earlier. Similarly, the R_{ct} is also decreased dramatically after etching, which increases the better charge transfer to the electrode from the electrolyte solution. Based on the comparative EIS study of 3DP MAX and 3DP-etched-MAX electrodes, it is confirmed that 3DP-etched-MAX shows better capacitive performance than 3DP MAX electrodes.

4. Conclusions

The study demonstrates the fabrication of bespoke MAX/PLA composite filament for FDM 3D printing followed by electrochemical etching to be utilized in different energy applications. The filament contains PLA, Ti_3AlC_2 MAX and PEG in mass ratio of 100:10:4, which provides desirable properties for filament extrusion and flexibility for 3D printing. After electrochemical etching, the 3DP-etched-MAX electrode showed promising overpotential for photo-electrochemical hydrogen evolution reaction (HER) and excellent capacitive performance to be used as a supercapacitor electrode. The fluoride-free etching of 3DP MAX electrode into 3DP-etched-MAX electrode added an advantage for large-scale production of MXene electrode for energy-related applications. The 3DP-etched-MAX electrode shows an overpotential of $\approx 351 \text{ mV}$ on light illumination 365 nm at the current density -10 mA cm^{-2} which is better than the other illuminated wavelength of 460 nm. Besides, the electrode shows an areal capacitance of $\approx 40.36 \text{ mF cm}^{-2}$ at the current density of $\approx 1.01 \text{ mA cm}^{-2}$. The work will pave the way for the fabrication of any MAX/PLA filament from the big family of discovered MAX so far for FDM 3D printing and electrochemically etching them to MXene electrodes for different applications like bio-sensing, electromagnetic interference shielding beyond energy conversion and storage applications.

CRediT authorship contribution statement

Shaista Nouseen: Conceptualization, Formal analysis, Data

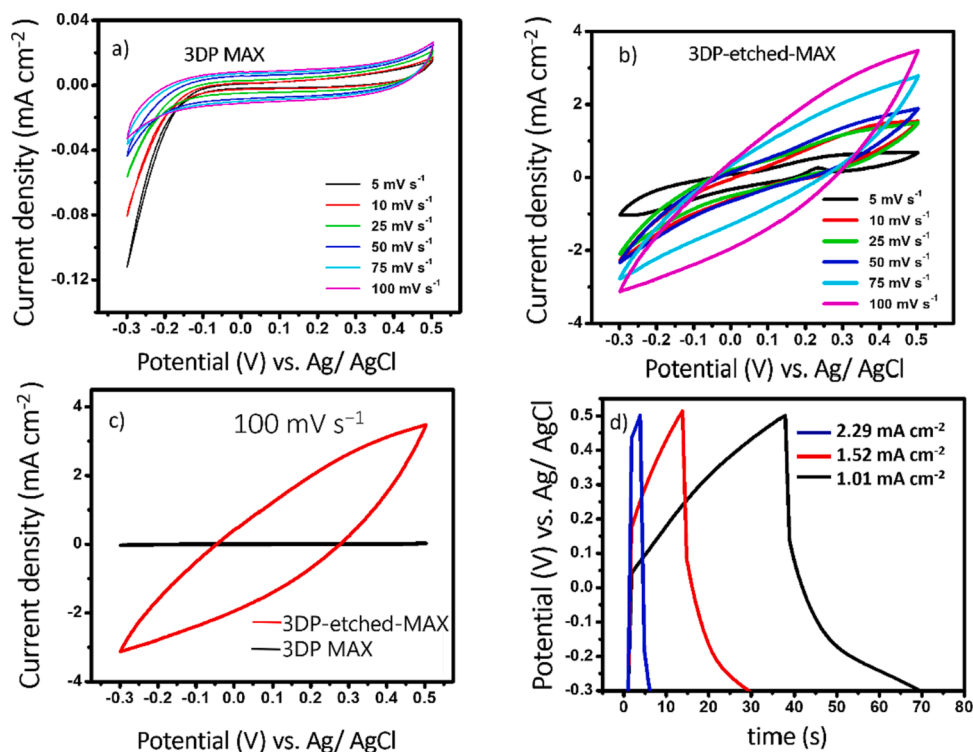


Fig. 7. The capacitance measurement of 3DP MAX and 3DP-etched-MAX electrodes is carried out in 1 M LiCl electrolyte in a three-electrode setup. (a) MAX electrode cyclic voltammetry studies with different scan rates. (b) 3DP-etched-MAX electrode cyclic voltammetry studies with different scan rates. (c) Comparison of 3DP MAX and 3DP-etched-MAX electrodes cyclic voltammetry studies with 100 mV s^{-1} scan rate. (d) Galvanostatic charge-discharge studies at different current density values.

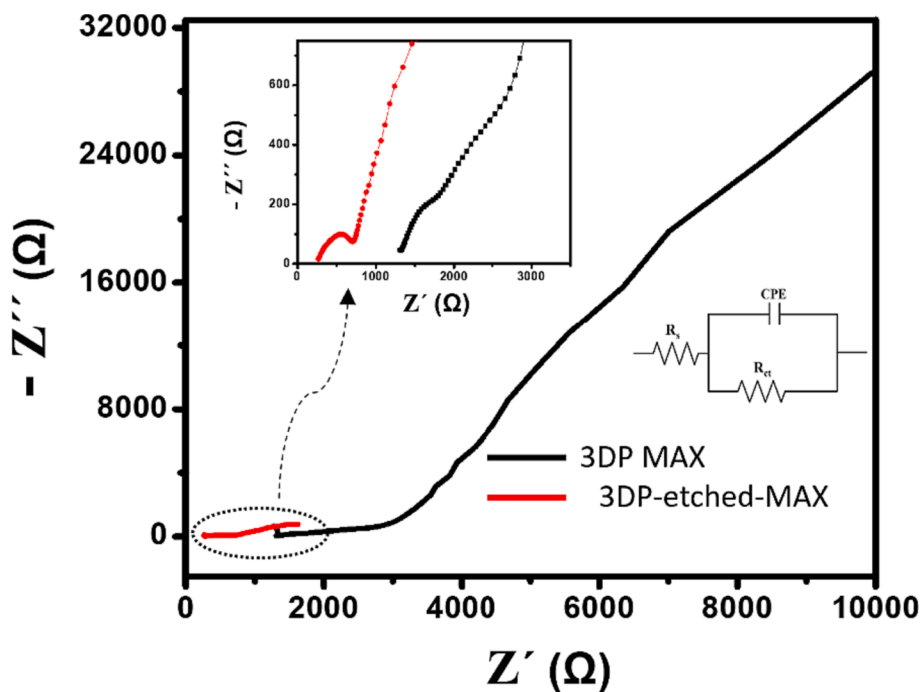


Fig. 8. Electrochemical impedance spectroscopy (EIS) study. Nyquist plot of 3DP MAX and 3DP-etched-MAX electrodes at frequency region of 1 MHz–0.01 Hz. Inset: magnified plot of the selected region and Randles circuit model for fitting the semicircle region.

curation, Investigation, Methodology, Validation, Visualization, Writing - original draft. **Kalyan Ghosh:** Supervision, Project administration, Conceptualization, Methodology, Formal analysis, Writing - review & editing. **Martin Pumera:** Supervision, Project administration, Funding acquisition, Conceptualization, Formal analysis, Writing - review &

editing.

Declaration of competing interest

The authors declare that they have no known competing financial

interests or personal relationships that could have appeared to influence the work reported in this paper.

Data availability

Data will be made available on request.

Acknowledgement

S.N. acknowledges the Internal Grant Agency of Mendel University in Brno, Faculty of AgriSciences, project No. AF-IGA2023-IP-059 and Mendel PhD talent. The work was supported by ERDF/ESF project TECHSCALE (No. CZ.02.01.01/00/22_008/0004587). This research was co-funded by the European Union under the REFRESH-Research Excellence For REgion Sustainability and High-tech Industries project number CZ.10.03.01/00/22_003/0000048 via the Operational Programme Just Transition. The material characterization was done with the support of the CzechNanoLab project at CEITEC Nano Research Infrastructure MEYS CR (LM2023051).

Appendix A. Supplementary material

Fig. S1 shows the CAD-designed electrodes for FDM 3D printing of MAX/PLA filament. Fig. S2 shows the chronoamperometry curve of Ti_3AlC_2 in 9 M HCl electrolyte. Fig. S3 shows the chronoamperometry curve of Ti_3AlC_2 in 4 M NaOH electrolyte. Fig. S4 show Energy-dispersive X-ray spectroscopy mapping of 3DP MAX and 3DP-etched-MAX electrode. Fig. S5 shows the UV spectra of the 3DP-etched-MAX electrode. Fig. S6 shows CV curves at different scan rates for the analysis of the double-layer capacitance CDL of the 3DP MAX and 3DP-etched-MAX electrodes. The XPS wide spectra atomic percentage calculation of 3DP MAX and 3DP-etched-MAX electrodes is given in Supporting Information Table S1. Supplementary information data of this article can be found online at <https://doi.org/10.1016/j.elecom.2023.107652>

References

- S.Y. Tee, K.Y. Win, W.S. Teo, L.D. Koh, S. Liu, C.P. Teng, M.Y. Han, Recent progress in energy-driven water splitting, *Adv. Sci.* 4 (5) (2017) 1600337, <https://doi.org/10.1002/advs.201600337>.
- S. Ng, J. Sturala, J. Vyskocil, P. Lazar, J. Martincova, J. Plutnar, M. Pumera, Two-dimensional functionalized germananes as photoelectrocatalysts, *ACS Nano* 15 (2021) 11681–11693, <https://doi.org/10.1021/acsnano.1c02327>.
- M. Sanna, S. Ng, J.V. Vaghasiya, M. Pumera, Fluorinated MAX phases for photoelectrochemical hydrogen evolution, *ACS Sustain. Chem. Eng.* 10 (2022) 2793–2801, <https://doi.org/10.1021/acssuschemeng.1c08133>.
- M. Sanna, K.A. Novčić, S. Ng, M. Černý, M. Pumera, The unexpected photoelectrochemical activity of MAX phases: the role of oxide impurities, *J. Mater. Chem. A* 11 (6) (2023) 3080–3090, <https://doi.org/10.1039/d2ta06929f>.
- S. Ng, K. Ghosh, J. Vyskocil, M. Pumera, Two-dimensional vanadium sulfide flexible graphite/polymer films for near-infrared photoelectrocatalysis and electrochemical energy storage, *Chem. Eng. J.* 435 (2022) 135131, <https://doi.org/10.1016/j.cej.2022.135131>.
- M. Sanna, S. Ng, M. Pumera, Layered transition metal selenophosphites for visible light photoelectrochemical production of hydrogen, *Electrochem. Commun.* 129 (2021) 107077, <https://doi.org/10.1016/j.elecom.2021.107077>.
- K.P. Akshay Kumar, O. Alduhaish, M. Pumera, Electrocatalytic activity of layered MAX phases for the hydrogen evolution reaction, *Electrochem. Commun.* 125 (2021) 106977, doi: 10.1016/j.elecom.2021.106977.
- C. Jellett, K. Ghosh, M.P. Browne, V. Urbanová, M. Pumera, Flexible graphite-poly (lactic acid) composite films as large-area conductive electrodes for energy applications, *ACS Appl. Energy Mater.* 4 (2021) 6975–6981, <https://doi.org/10.1021/acsaem.1c01047>.
- M.P. Browne, E. Redondo, M. Pumera, 3D printing for electrochemical energy applications, *Chem. Rev.* 120 (2020) 2783–2810, <https://doi.org/10.1021/acs.chemrev.9b00783>.
- W. Gao, C. Iffelsberger, M. Pumera, Dual polymer engineering enables high-performance 3D printed Zn-organic battery cathodes, *Appl. Mater. Today* 28 (2022) 101515, <https://doi.org/10.1016/j.apmt.2022.101515>.
- S.P. Sreenilayam, I. Ul Ahad, V. Nicolosi, D. Brabazon, MXene materials based printed flexible devices for healthcare, biomedical and energy storage applications, *Mater. Today* 43 (2021) 99–131, <https://doi.org/10.1016/j.mattod.2020.10.025>.
- K. Ghosh, S. Ng, C. Iffelsberger, M. Pumera, 2D MoS_2 /carbon/poly(lactic acid) filament for 3D printing: photo and electrochemical energy conversion and storage, *Appl. Mater. Today* 26 (2022) 101301, <https://doi.org/10.1016/j.apmt.2021.101301>.
- K. Ghosh, S. Ng, C. Iffelsberger, M. Pumera, Inherent impurities in graphene/poly(lactic acid) filament strongly influence on the capacitive performance of 3D-printed electrode, *Chem. Eur. J.* 26 (2020) 15746–15753, <https://doi.org/10.1002/chem.202004250>.
- K. Ghosh, M. Pumera, MXene and MoS_{3-x} coated 3D-printed hybrid electrode for solid-state asymmetric supercapacitor, *Small Methods* 5 (2021) 2100451, <https://doi.org/10.1002/smt.202100451>.
- C.W. Foster, M.P. Down, Y. Zhang, X. Ji, S.J. Rowley-Neale, G.C. Smith, P.J. Kelly, C.E. Banks, 3D printed graphene based energy storage devices, *Sci. Rep.* 7 (2017) 42233, <https://doi.org/10.1038/srep42233>.
- K.P. Akshay Kumar, K. Ghosh, O. Alduhaish, M. Pumera, Dip-coating of MXene and transition metal dichalcogenides on 3D-printed nanocarbon electrodes for the hydrogen evolution reaction, *Electrochem. Commun.* 122 (2021) 106890, <https://doi.org/10.1016/j.elecom.2020.106890>.
- C. Reyes, R. Somogyi, S. Niu, M.A. Cruz, F. Yang, M.J. Catenacci, C.P. Rhodes, B. J. Wiley, Three-dimensional printing of a complete lithium ion battery with fused filament fabrication, *ACS Appl. Energy Mater.* 1 (2018) 5268–5279, <https://doi.org/10.1021/acsaem.8b00885>.
- A. Maurel, M. Courty, B. Fleutot, H. Tortajada, K. Prashantha, M. Armand, S. Grugeon, S. Panier, L. Dupont, Highly loaded graphite-poly(lactic acid) composite-based filaments for lithium-ion battery three-dimensional printing, *ACS Chem. Mater.* 30 (2018) 7484–7493, <https://doi.org/10.1021/acs.chemmater.8b02062>.
- J.P. Hughes, P.L. Dos Santos, M.P. Down, C.W. Foster, J.A. Bonacin, E.M. Keefe, S. J. Rowley-Neale, C.E. Banks, Single step additive manufacturing (3D printing) of electrocatalytic anodes and cathodes for efficient water splitting, *Sustain. Energy Fuels* 4 (2019) 302–311, <https://doi.org/10.1039/c9se00679f>.
- A. Maurel, S. Grugeon, B. Fleutot, M. Courty, K. Prashantha, H. Tortajada, M. Armand, S. Panier, L. Dupont, Three-dimensional printing of a LiFePO_4 /graphite battery cell via fused deposition modeling, *Sci. Rep.* 9 (2019) 18031, <https://doi.org/10.1038/s41598-019-54518-y>.
- J. Pang, R.G. Mendes, A. Bachmatiuk, L. Zhao, H.Q. Ta, T. Gemming, H. Liu, Z. Liu, M.H. Rummeli, Applications of 2D MXenes in energy conversion and storage systems, *Chem. Soc. Rev.* 48 (2019) 72–133, <https://doi.org/10.1039/c8cs00324f>.
- K. Li, M. Liang, H. Wang, X. Wang, Y. Huang, J. Coelho, S. Pinilla, Y. Zhang, F. Qi, V. Nicolosi, Y. Xu, 3D MXene architectures for efficient energy storage and conversion, *Adv. Funct. Mater.* 30 (2020) 2000842, <https://doi.org/10.1002/adfm.202000842>.
- Y. Chen, H. Yang, Z. Han, Z. Bo, J. Yan, K. Cen, K.K. Ostrikov, MXene-based electrodes for supercapacitor energy storage, *Energy Fuels* 36 (2022) 2390–2406, <https://doi.org/10.1021/acs.energyfuels.1c04104>.
- L. Liao, D. Jiang, K. Zheng, M. Zhang, J. Liu, Industry-scale and environmentally stable $\text{Ti}_3\text{C}_2\text{T}_x$ MXene based film for flexible energy storage devices, *Adv. Funct. Mater.* 31 (2021) 2103960, <https://doi.org/10.1002/adfm.202103960>.
- H. Li, X. Li, J. Liang, Y. Chen, Hydrous RuO_2 -decorated MXene coordinating with silver nanowire inks enabling fully printed micro-supercapacitors with extraordinary volumetric performance, *Adv. Energy Mater.* 9 (15) (2019) 1803987, <https://doi.org/10.1002/aenm.201803987>.
- W. Yang, J. Yang, J.J. Byun, F.P. Moissinac, J. Xu, S.J. Haigh, M. Domingos, M.A. Bissett, R.A.W. Dryfe, S. Barg, 3D printing of freestanding MXene architectures for current-collector-free supercapacitors, *Adv. Mater.* 31.37 (2019) 1902725, doi: 10.1002/adma.201902725.
- K. Ghosh, M. Pumera, Free-standing electrochemically coated MoS_x based 3D-printed nanocarbon electrode for solid-state supercapacitor application, *Nanoscale* 13 (2021) 5744–5756, <https://doi.org/10.1039/d0nr06479c>.
- J. Pang, B. Chang, H. Liu, W. Zhou, Potential of MXene-based heterostructures for energy conversion and storage, *ACS Energy Lett.* 7 (2022) 78–96, <https://doi.org/10.1021/acsenerylett.1c02132>.
- M. Alhabeib, K. Maleski, B. Anasori, P. Lelyukh, L. Clark, S. Sin, Y. Gogotsi, Guidelines for synthesis and processing of two-dimensional titanium carbide ($\text{Ti}_3\text{C}_2\text{T}_x$ MXene), *ACS Chem. Mater.* 29 (2017) 7633–7644, <https://doi.org/10.1021/acs.chemmater.7b02847>.
- C.E. Shuck, A. Sarycheva, M. Anayee, A. Levitt, Y. Zhu, S. Uzun, V. Balitskiy, V. Zhorodna, O. Gogotsi, Y. Gogotsi, Scalable synthesis of $\text{Ti}_3\text{C}_2\text{T}_x$ MXene, *Adv. Eng. Mater.* 22 (3) (2020) 1901241, <https://doi.org/10.1002/adem.201901241>.
- M. Naguib, M.W. Barsoum, Y. Gogotsi, Ten years of progress in the synthesis and development of MXenes, *Adv. Mater.* 33 (2021), <https://doi.org/10.1002/adma.202103393>.
- C.B. Cockreham, V.G. Goncharov, E. Hammond-Pereira, M.E. Reece, A. C. Strzelecki, W. Xu, S.R. Saunders, H. Xu, X. Guo, D. Wu, Energetic stability and interfacial complexity of $\text{Ti}_3\text{C}_2\text{T}_x$ MXenes synthesized with HF/HCl and CoF_2/HCl as etching agents, *ACS Appl. Mater. Interfaces* 14 (2022) 41542–41554, <https://doi.org/10.1021/acsaami.2c09669>.
- A.D. Handoko, K.D. Fredrickson, B. Anasori, K.W. Convey, L.R. Johnson, Y. Gogotsi, A. Vojvodic, Z.W. Seh, Tuning the basal plane functionalization of two-dimensional metal carbides (MXenes) to control hydrogen evolution activity, *ACS Appl. Energy Mater.* 1 (2018) 173–180, <https://doi.org/10.1021/acsaem.7b00054>.
- T. Wu, P.R.C. Kent, Y. Gogotsi, D.E. Jiang, How water attacks MXene, *ACS Chem. Mater.* 34 (2022) 4975–4982, <https://doi.org/10.1021/acs.chemmater.2c00224>.
- S. Huang, V.N. Mochalin, Hydrolysis of 2D transition-metal carbides (MXenes) in colloidal solutions, *Inorg. Chem.* 58 (2019) 1958–1966, <https://doi.org/10.1021/acs.inorgchem.8b02890>.

- [36] Y. Chae, S.J. Kim, S.Y. Cho, J. Choi, K. Maleski, B.J. Lee, H.T. Jung, Y. Gogotsi, Y. Lee, C.W. Ahn, An investigation into the factors governing the oxidation of two-dimensional Ti_3C_2 MXene, *Nanoscale* 11 (2019) 8387–8393, <https://doi.org/10.1039/c9nr00084d>.
- [37] V. Natu, R. Pai, M. Sokol, M. Carey, V. Kalra, M.W. Barsoum, 2D $\text{Ti}_3\text{C}_2\text{T}_x$ MXene synthesized by water-free etching of Ti_3AlC_2 in polar organic solvents, *Chem* 6 (2020) 616–630, <https://doi.org/10.1016/j.chempr.2020.01.019>.
- [38] K.A. Novčić, C. Iffelsberger, M. Pumera, Layered MAX phase electrocatalyst activity is driven by only a few hot spots, *J. Mater. Chem. A* 10 (2022) 3206–3215, <https://doi.org/10.1039/d1ta06419c>.
- [39] Y.J. Kim, S.J. Kim, D. Seo, Y. Chae, M. Anayee, Y. Lee, Y. Gogotsi, C.W. Ahn, H. T. Jung, Etching mechanism of monoatomic aluminum layers during MXene synthesis, *ACS Chem. Mater.* 33 (2021) 6346–6355, <https://doi.org/10.1021/acs.chemmater.1c01263>.
- [40] R. Ramírez, A. Melillo, S. Osella, A.M. Asiri, H. Garcia, A. Primo, Green, HF-free synthesis of MXene quantum dots and their photocatalytic activity for hydrogen evolution, *Small Methods* 7 (2023) 2300063, <https://doi.org/10.1002/smt.202300063>.
- [41] R.M. Ronchi, J.T. Arantes, S.F. Santos, Synthesis, structure, properties and applications of MXenes: current status and perspectives, *Ceram. Int.* 45 (2019) 18167–18188, <https://doi.org/10.1016/j.ceramint.2019.06.114>.
- [42] I.-W.-P. Chen, A.A. Kashale, Y.-H. Pan, Hydrofluoric acid-free synthesis of $\text{Ti}_3\text{C}_2\text{T}_x$ MXene nanostructures for energy applications, *ACS Appl. Nano Mater.* 6 (3) (2023) 1985–1995, <https://doi.org/10.1021/acsanm.2c04948>.
- [43] S.Y. Pang, Y.T. Wong, S. Yuan, Y. Liu, M.K. Tsang, Z. Yang, H. Huang, W.T. Wong, J. Hao, Universal strategy for HF-free facile and rapid synthesis of two-dimensional MXenes as multifunctional energy materials, *J. Am. Chem. Soc.* 141 (2019) 9610–9616, <https://doi.org/10.1021/jacs.9b02578>.
- [44] W. Sun, S.A. Shah, Y. Chen, Z. Tan, H. Gao, T. Habib, M. Radovic, M.J. Green, Electrochemical etching of Ti_2AlC to Ti_2CT : X (MXene) in low-concentration hydrochloric acid solution, *J. Mater. Chem. A* 5 (2017) 21663–21668, <https://doi.org/10.1039/c7ta05574a>.
- [45] J. Chen, M. Chen, W. Zhou, X. Xu, B. Liu, W. Zhang, C. Wong, Simplified synthesis of fluoride-free $\text{Ti}_3\text{C}_2\text{T}_x$ via electrochemical etching toward high-performance electrochemical capacitors, *ACS Nano* 16 (2022) 2461–2470, <https://doi.org/10.1021/acsnano.1c09004>.
- [46] T. Li, L. Yao, Q. Liu, J. Gu, R. Luo, J. Li, X. Yan, W. Wang, P. Liu, B. Chen, W. Zhang, W. Abbas, R. Naz, D. Zhang, Fluorine-free synthesis of high-purity $\text{Ti}_3\text{C}_2\text{T}_x$ (T=OH, O) via alkali treatment, *Angew. Chemie* 130 (2018) 6223–6227, <https://doi.org/10.1002/ange.201800887>.
- [47] S. Yang, P. Zhang, F. Wang, A.G. Ricciardulli, M.R. Lohe, P.W.M. Blom, X. Feng, Fluoride-free synthesis of two-dimensional titanium carbide (MXene) using a binary aqueous system, *Angew. Chemie* 130 (2018) 15717–15721, <https://doi.org/10.1002/ange.201809662>.
- [48] R.A. Vaia, A. Jawaid, A. Hassan, G. Neher, D. Nepal, R. Pachter, W. Joshua Kennedy, S. Ramakrishnan, Halogen etch of Ti_3AlC_2 MAX phase for mxene fabrication, *ACS Nano* 15 (2021) 2771–2777, <https://doi.org/10.1021/acsnano.0c08630>.
- [49] D. Wang, C. Zhou, A.S. Filatov, W. Cho, F. Lagunas, M. Wang, S. Vaikuntanathan, C. Liu, R.F. Klie, D. V Talapin, Direct synthesis and chemical vapor deposition of 2D carbide and nitride MXenes, *Science* 379 (6638) (2023) 1242–1247, n.d., <http://www.science.org>.
- [50] M. Li, J. Lu, K. Luo, Y. Li, K. Chang, K. Chen, J. Zhou, J. Rosen, L. Hultman, P. Eklund, P.O.Å. Persson, S. Du, Z. Chai, Z. Huang, Q. Huang, Element replacement approach by reaction with Lewis acidic molten salts to synthesize nanolaminated MAX phases and MXenes, *J. Am. Chem. Soc.* 141 (2019) 4730–4737, <https://doi.org/10.1021/jacs.9b00574>.
- [51] Y. Li, H. Shao, Z. Lin, J. Lu, L. Liu, B. Duployer, P.O.Å. Persson, P. Eklund, L. Hultman, M. Li, K. Chen, X.H. Zha, S. Du, P. Rozier, Z. Chai, E. Raymundo-Piñero, P.L. Taberna, P. Simon, Q. Huang, A general Lewis acidic etching route for preparing MXenes with enhanced electrochemical performance in non-aqueous electrolyte, *Nat. Mater.* 19 (2020) 894–899, <https://doi.org/10.1038/s41563-020-0657-0>.
- [52] D.M. Wirth, M.J. Sheaff, J.V. Waldman, M.P. Symcox, H.D. Whitehead, J.D. Sharp, J.R. Doerfler, A.A. Lamar, G. Leblanc, Electrolysis activation of fused-filament-fabrication 3D-printed electrodes for electrochemical and spectroelectrochemical analysis, *Anal. Chem.* 91 (2019) 5553–5557, <https://doi.org/10.1021/acs.analchem.9b01331>.
- [53] F.J. Burger, V.F.G. Tull, Gas content and electrolytic etching behaviour of aluminium, *Nature* 172 (1953) 729–730, <https://doi.org/10.1038/172729a0>.
- [54] J. Bernard, M. Chatenet, F. Dalard, Understanding aluminum behaviour in aqueous alkaline solution using coupled techniques, *Electrochim. Acta* 52 (2006) 86–93, <https://doi.org/10.1016/j.electacta.2006.03.076>.
- [55] T.S. Mathis, K. Maleski, A. Goad, A. Sarycheva, M. Anayee, A.C. Foucher, K. Hantanasirisakul, C.E. Shuck, E.A. Stach, Y. Gogotsi, Modified MAX phase synthesis for environmentally stable and highly conductive Ti_3C_2 MXene, *ACS Nano* 15 (2021) 6420–6429, <https://doi.org/10.1021/acsnano.0c08357>.
- [56] Q. Zhang, J. He, X. Fu, S. Xie, R. Fan, H. Lai, W. Cheng, P. Ji, J. Sheng, Q. Liao, W. Zhu, H. Li, Fluorine-free strategy for hydroxylated $\text{Ti}_3\text{C}_2/\text{Ti}_3\text{AlC}_2$ catalysts with enhanced aerobic oxidative desulfurization and mechanism, *Chem. Eng. J.* 430 (2022) 132950, <https://doi.org/10.1016/j.cej.2021.132950>.
- [57] L.Å. Naslund, P.O.Å. Persson, J. Rosen, X-ray photoelectron spectroscopy of Ti_3AlC_2 , $\text{Ti}_3\text{C}_2\text{T}_x$, and TiC provides evidence for the electrostatic interaction between laminated layers in max-phase materials, *J. Phys. Chem. C* 124 (2020) 27732–27742, <https://doi.org/10.1021/acs.jpcc.0c07413>.
- [58] W. Qiang, X. Qu, C. Chen, L. Zhang, D. Sun, Ti_3C_2 MXene derived (001) $\text{TiO}_2/\text{Ti}_3\text{C}_2$ heterojunctions for enhanced visible-light photocatalytic degradation of tetracycline, *Mater. Today Commun.* 33 (2022) 104216, <https://doi.org/10.1016/j.mtcomm.2022.104216>.
- [59] V. Natu, M. Benchakar, C. Canaff, A. Habrioux, S. Céli er, M.W. Barsoum, A critical analysis of the X-ray photoelectron spectra of $\text{Ti}_3\text{C}_2\text{T}_x$ MXenes, *Mater.* 4 (2021) 1224–1251, <https://doi.org/10.1016/j.matt.2021.01.015>.
- [60] R. Kang, Z. Zhang, L. Guo, J. Cui, Y. Chen, X. Hou, B. Wang, C. Te Lin, N. Jiang, J. Yu, Enhanced thermal conductivity of epoxy composites filled with 2D transition metal carbides (MXenes) with ultralow loading, *Sci. Rep.* 9 (2019) 9135, <https://doi.org/10.1038/s41598-019-45664-4>.
- [61] A.M. Jastrz bska, A. Szuplewska, A. Rozmyslowska-Wojciechowska, M. Chudy, A. Olszyna, M. Birowska, M. Popielski, J.A. Majewski, B. Scheibe, V. Natu, M. W. Barsoum, On tuning the cytotoxicity of Ti_3C_2 (MXene) flakes to cancerous and benign cells by post-delamination surface modifications, *2d Mater.* 7 (2020) 025018, <https://doi.org/10.1088/2053-1583/ab6a60>.
- [62] J. He, P. Wu, L. Chen, H. Li, M. Hua, L. Lu, Y. Wei, Y. Chao, S.S. Zhou, W. Zhu, H. Li, Dynamically-generated TiO_2 active site on MXene Ti_3C_2 : boosting reactive desulfurization, *Chem. Eng. J.* 416 (2021) 129022, <https://doi.org/10.1016/j.cej.2021.129022>.
- [63] C. Zhou, X. Wang, H. Luo, L. Deng, S. Wei, Y. Zheng, Q. Jia, J. Liu, Rapid and direct growth of bipyramid TiO_2 from $\text{Ti}_3\text{C}_2\text{T}_x$ MXene to prepare $\text{Ni}/\text{TiO}_2/\text{C}$ heterogeneous composites for high-performance microwave absorption, *Chem. Eng. J.* 383 (2020) 123095, <https://doi.org/10.1016/j.cej.2019.123095>.
- [64] J.X. Yang, W.B. Yu, C.F. Li, W. Da Dong, L.Q. Jiang, N. Zhou, Z.P. Zhuang, J. Liu, Z. Y. Hu, H. Zhao, Y. Li, L. Chen, J. Hu, B.L. Su, PtO nanodots promoting Ti_3C_2 MXene in-situ converted $\text{Ti}_3\text{C}_2/\text{TiO}_2$ composites for photocatalytic hydrogen production, *Chem. Eng. J.* 420 (2021) 129695, <https://doi.org/10.1016/j.cej.2021.129695>.
- [65] E. Satheshkumar, T. Makaryan, A. Melikyan, H. Minassian, Y. Gogotsi, M. Yoshimura, One-step solution processing of Ag, Au and Pd@MXene hybrids for SERS, *Sci. Rep.* 6 (2016) 32049, <https://doi.org/10.1038/srep32049>.
- [66] A. Iqbal, N.M. Hamdan, Investigation and optimization of mxene functionalized mesoporous titania films as efficient photoelectrodes, *Materials* 14 (21) (2021) 6292, <https://doi.org/10.3390/ma14216292>.